ACS APPLIED MATERIALS & INTERFACES

Research Article

www.acsami.org

Automatically Acquired Broadband Plasmonic-Metamaterial Black Absorber during the Metallic Film-Formation

Zhengqi Liu,*[,†] Xiaoshan Liu,[†] Shan Huang,[†] Pingping Pan,[†] Jing Chen,[#] Guiqiang Liu,*[,†] and Gang Gu[†]

[†]Laboratory of Nanomaterials and Sensors, College of Physics and Communication Electronics, Provincial Key Laboratory of Optoelectronic and Telecommunication, Jiangxi Normal University, Nanchang 330022, China

[#]College of Electronic Science and Engineering, Nanjing University of Posts and Telecommunications, Nanjing 210023, China

ABSTRACT: Broadband electromagnetic wave absorbers are highly desirable in numerous applications such as solar-energy harvesting, thermo-photovoltaics, and photon detection. The aim to efficiently achieve ultrathin broadband absorbers with high-yield and low-cost fabrication process has long been pursued. Here, we theoretically propose and experimentally demonstrate a unique broadband plasmonic-metamaterial absorber by utilizing a sub-10 nm meta-surface film structure to replace the precisely designed metamaterial crystal in the common metal−dielectric−metal absorbers. The unique ultrathin meta-surface can be automatically obtained during the metal film formation process. Spectral bandwidth with absorbance above 80% is up to 396 nm, where the full absorption width at half-maximum is about 92%. The average value of absorbance across the whole spectral range of 370−880 nm reaches 83%. These super absorption properties can be attributed to the particle plasmon resonances and plasmon near-field coupling by the automatically formed metallic nanoparticles as well as the plasmon polaritons of the metal film with the induced plasmonic magnetic resonances occurring between the top meta-surface and the bottom metal mirror. This method is quite simple, cost-effective for large-area fabrication, and compatible with current industrial methods for microelectro-mechanical systems, which makes it an outstanding candidate for advanced high-efficiency absorber materials.

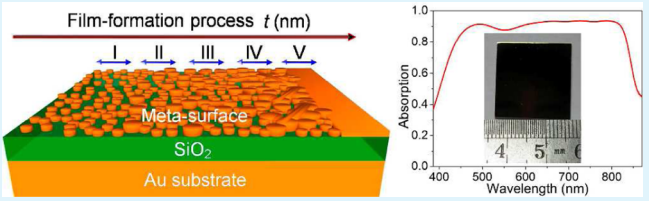

KEYWORDS: *particle plasmon resonances, plasmon near-field coupling, plasmonic-metamaterial absorber, metal film formation, deposition*

INTRODUCTION

Electromagnetic absorbers have wide application in spectroscopy[1] and sensing,[2,3] solar cell[4] and thermal emitters,[5] and photon detection.[6] Among the electromagnetic structures, metamaterials, which are composed of subwavelength scale resonators with customized electronic and magnetic response, have emerged as compelling candidates for optical light absorbers. Since its first publication in 2008,[7] the electromagnetic wave absorbers have been intensively investigated from microwave to optical frequencies. By utilizing electric ring resonators or metal−insulator−metal (MIM) cavities,[8−11] high absorption can be observed in a narrow frequency range due to the intrinsic electronic and magnetic resonances occurring synchronously at a certain wavelength.[7,10,11] These narrowband absorbers reflect a large amount of incident light within a broad frequency range, thus limiting their applications. To overcome this limitation, great efforts have been made in the previous decade, and several methods have been proposed such as mixing multiple resonators with the resonances at different frequencies,[12−14] exciting phase resonances to divide the absorption band into multiple sub-bands,[15] or employing tapered anisotropic metamaterial waveguide to make light slow,[16−18] and so on.[19−21] Based on the concept of the collective effect of multiple distinct oscillators or the absorption subsystems within the same unit cell, the conventional narrowband absorption could be extremely expanded and become a superbroadband absorption spectrum. However, accompanied by the broadening of the absorption band, the related processing techniques inevitably become more complicated. Especially, it is still a great challenge in experiments to realize some excellent absorbing devices proposed by theorists, which is limited by the processing techniques available today, especially for those working in the optical frequency. Furthermore, future industrialization requires a simple and low-cost technique to fabricate large-area metallic subwavelength structures.[10,11] Thereby, it is highly desirable to exploit some new routes to overcome the formidable challenges, including the main issues of high fabrication requirements, energy consumption, and production cost, which is significant in finding high-performance solar absorbers.[10,11]

Nearly ideal plasmonic absorbers have also been demonstrated for the visible, near-infrared, and mid-infrared spectral regimes by using nonresonant nanomaterials, including metallic nanoparticles,[22,23] metal−dielectric microstructures,[24,25] and vertically aligned single-walled carbon nanotubes.[26] For instance, by tailoring the plasmonic modes of a metal−dielectric−metal structure consisting of gold nanogratings and

Received: January 4, 2015
Accepted: February 13, 2015
Published: February 13, 2015

DOI: 10.1021/acsami.5b00056
ACS Appl. Mater. Interfaces 2015, 7, 4962−4968

silver nanocubes, a large multiplicative enhancement of absorption properties was achieved in the visible frequencies.[27] Nevertheless, it is very difficult to fabricate this kind of absorber over a large area since high-precision fabrication techniques including electronic beam lithography are needed. These technical issues inevitably limit its further application. In addition, these solutions offer limited flexibility to tailor the wavelength range and absorption bandwidth. In addition, achieving complete absorption of visible light with a minimal amount of material is very interesting for many applications including solar energy conversion to fuel and electricity, where benefits in conversion efficiency and economy can be achieved. By combining the block copolymer lithography and atomic layer deposition, it is very effective to tune the optical properties of a self-assembled plasmonic Au dot array at the atomic scale in the plasmonic absorber/spacer/reflector structure, which exhibits excellent visible light absorption up to 93.4% with quite low consumption of Au.[28] However, the high absorption only occurs within a narrowband wavelength range due to the single plasmon resonance excited by the plasmonic grating structure. Therefore, although many efforts have been made to this point, the achievement of high-performance absorbers with a wide working wavelength range by using a minimal amount of material in conjunction with a simple and cost-effective method is still a challenge.

In this paper, we demonstrate the design, fabrication, and characterization of a novel automatically acquired ultrathin broadband plamonic-metamaterial absorber (PMA) during the metallic film-formation process. The full-absorption bandwidth with absorbance (A) above 80% is up to 396 nm from 439 to 835 nm. The maximal A is up to 93% and the full absorption width at the half-maximum is about 92%. Across the broad wavelength range of 370−880 nm in the entire spectrum, the average value of absorbance is equal to 83%. These absorption properties mainly benefit from the multiple plasmon resonances of the sputtered metallic nanoparticles with wide size distribution and the strong plasmon near-field coupling resonance by the metallic nanoparticles located in close proximity, and the plasmon polariton effects occurring between the top meta-surface and the bottom metal mirror. Our technique is quite simple, cost-effective, and straightforward, which makes it an outstanding candidate for advanced high-efficiency absorber materials. Furthermore, the absorber layer of the metallic film is within a norminal thickness of less than 10 nm, which could be useful for the efficient conversion of solar energy to fuel and electricity.[28] These optical features and structural characteristics provide the PMA with great potential to be used in solar energy and thermophotovoltaics.[4,29−31]

EXPERIMENTAL AND SIMULATION SECTION

Broadband PMA Fabrication and Characterization. Fabrication of the PMA began by depositing a 100 nm Au layer on a clean quartz substrate by argon ion beam sputtering (Model 682 PECS, Gatan Corp.) under a situation within a vacuum of 5×10^{-6} Torr (1 Torr = 133 Pa) at a rate of 0.67 A s^{-1}. The SiO_2 spacer layer coated on this opaque Au mirror was then obtained via the same deposition system by rotating the sputtering target from the gold to the quartz and depositing with a rate of 0.83 A s^{-1}. The top meta-surface structure of the PMA was prepared by the same system by rotating the sputtering target to the gold and repeated the deposition process. The thicknesses and sizes of the produced structures were measured by field-emission scanning electron microscopy (S-4800). A tungsten halogen lamp with a gold reflector providing a wavelength range of 370−880 nm and a peak power of 150 W was used as a light source. The optical properties of the PMAs were characterized using a grating spectrophotometer (Omni-λ500) together with an integration sphere under a spectral range of 200−1000 nm. The oblique incidence measurements were made using a custom-designed setup of a specular reflection accessory. The measured reflection was referenced to a Au mirror to determine the absolute reflectivity, R. Since the transmission channel is completely canceled by the opaque metal mirror, the absorption according to $A = 1 - R - T$ was determined directly to be $A = 1 - R$.

Electromagnetic Simulation. Simulations were performed using three-dimensional (3D) finite-difference time-domain method.[32] 3D simulations of two cube periods with periodic x- and y-boundaries and perfectly matched layer z-boundaries were used for modeling the gold cubes. A Gauss light source with a wide pulse wavelength range of 350−1000 nm was used for illumination and a $1 \times 1 \times 1$ nm^3 mesh unit cell was used across the entire simulation region for both cubes and other structures. The complex dielectric constants of gold are taken from measured data and described by the Drude model $\varepsilon_m = \varepsilon_\infty - \omega_p^2/[\omega(\omega + i\gamma)]$,[33] where ω_p is the bulk plasmon frequency of the Au, ω is the angle frequency of the incident wave, and γ represents the damping rate which characterizes the ohmic absorption loss. The values of the ε_∞, ω_p, and γ in the Drude model are 9.84, 9.01 eV, and 0.072 eV, respectively. These proper setting values could satisfactorily reproduce the experimental values of gold in the range of 0.8−5.0 eV.

RESULTS AND DISCUSSION

Electromagnetic Optimization Methodology and Fabrication Process. In general, our broadband PMA is mainly composed of a three-layer metallo−dielectric−metallo stack, which is similar to the conventional MIM metamaterial absorbers.[7−9] The bottom 100-nm-thick metal mirror and the dielectric spacer film are typical structures, which could be fabricated in large scale with the standard sputtering method.[24,34] Usually, for conventional MIM metamaterial absorbers, the top layer of the uniformly packed metallic unit cells especially for the cells containing a series of different structural sizes of subsystems are highly difficult to fabricate.[10,11] Also, electron beam lithography or focused ion beam milling is commonly utilized to produce such high-precision structures, which leads to high cost and high consumption.[35−37] In sharp contrast, in our case, the top active layer is just an automatically formed meta-surface, which can be fabricated straightforwardly during the metal film-formation process, suggesting that our technique is very simple, low-cost, and highly efficient. The only key technical thing needed here is to set the deposition procedure before the automatic sputtering deposition. These unique features promote this PMA as a feasible material for mass production of the broadband absorber.

The reason for us to propose this motif for broadband absorbers is based on the inspiration from the significant findings in the previous reports.[7,10−14] Since the first landmark report of the metamaterial absorber with near-unity absorption but with a narrowband spectral range,[7] various efforts have been made to improve the absorption bandwidth. The simplest as well as the most direct method is to embrace multiple resonances working at distinct frequencies within the same unit

DOI: 10.1021/acsami.5b00056
ACS Appl. Mater. Interfaces 2015, 7, 4962−4968

cell by using the concept of the collective effect of multiple distinct oscillators.[10−14] Nevertheless, it inevitably increases the difficulty of the structural fabrication, and even leads to the impossibility of real fabrication via the current technique. So, the question here is whether there is a much easier way to produce multiple resonators involved in fewer procedures. Indeed, there are several ways including the metallic physical vapor deposition, which could produce a series of plasmonic resonators within one fabrication process due to the deposited metallic nanoparticles with a wide size distribution.[38−43] The different metallic nanoparticles could support the corresponding resonances occurring in the spectrum and overlap with each other, and therefore produce a broadened absorption spectrum.

In addition, between the adjacent metallic nanoparticles, strong plasmon near-field coupling effect could be excited, which has been theoretically and experimentally demonstrated in the previous reports by Prof. Nordland and coauthors.[44−47] It is well-known that the metallic nanoparticle arrays with strong plasmon near-field coupling could produce interesting optical properties of broadband electromagnetic field trapping and confinement.[48,49] These novel features have been widely used in the areas of surface enhanced spectroscopy,[39,44] surface enhanced metal film transparency,[50] surface enhanced sensing,[51−55] and biomaterial detection.[56] Nevertheless, far less attention has been focused on the investigations in the broadband electromagnetic wave absorption.

Here, we propose and demonstrate a black absorber by utilizing a unique meta-surface, which is automatically acquired during the deposited metal film-formation process. Accompanied by the sputtering deposition process, interestingly and importantly, the metallic nanoparticles show a continuous increase in size and simultaneously lead to the formation of the ultrasmall gaps between adjacent nanoparticles. As a result, strong plasmon near-field coupling effects and multiple particle plasmon resonances could be excited in this metallic film structure, resulting in a large multiplicative enhancement of absorption properties across a broad spectral range.

Figure 1a shows the schematic diagram of the proposed structure and the formation of a metal film during the sputtering deposition. For this work, structures were optimized

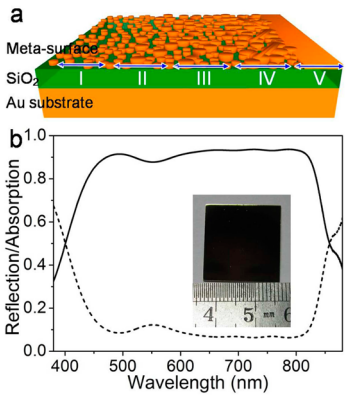

Figure 1. (a) Schematic of the metallic film-formation and building of the PMA structure by controlling the sputtering process. (b) Absorption (solid line) and reflection (dashed line) spectrum of the achieved PMA. Thicknesses of the top Au metal-surface film, SiO_2 spacer, and the bottom Au substrate are 7, 40, and 100 nm, respectively. The inset in (b) presents the optical photo of the PMA with the size of 2 × 2 cm^2.

using the noble metal with low reactivity, gold (Au), for both the ground plane and the meta-surface layer. Silica (SiO_2) was selected for the dielectric layer. Thrice-repeated deposition processes were performed to form the bottom metal mirror, the middle spacer, and the top meta-surface one after another. During the film formation process (Figure 1a), the deposited nanoparticles (nanocrystals, I) are of small size. By increasing the deposition time, the further deposited nanoparticles contact the former ones and then grow to large nanoparticles (II). Afterwards, the nanoparticles could grow and come into contact with each other, which spontaneously creates nanoclusters (III) from discrete nanoparticles. Then, with further deposition of nanoparticles (I) onto these formed nanoclusters (III) and voids, the porous film (IV) and the complete metal film (V) could be formed. These metallic film structures could be artificially tuned by the deposition characteristics such as deposition time.[24,40]

Structural Features and Broadband Absorption. The structural features of the PMA are displayed in Figure 1a. The ground metal mirror thickness was fixed to 100 nm, which is several times larger than the skin depth for Au. Due to the ultrathin film with irregular geometry structure, a norminal thickness is used for the meta-surface.[24,40] The norminal thickness of the preformation film is obtained by multiplying the deposition time with the deposition rate. Here, the nominal thickness ranges for the metal film-formation process (I to V in Figure 1a) are 0−2 nm, 3−5 nm, 6−8 nm, 9−11 nm, and >12 nm, respectively.

The normal incidence absorbance is determined from $A = 1 - R$ (where $T = 0$). The absorption spectrum (Figure 1b) shows that the minimum absorption remains above 80% in the spectral range from 439 to 835 nm (bandwidth up to 396 nm) and the full absorption width at the half-maximum is up to 92%. In addition, although the structure is only used with a 7 nm gold meta-surface, the achieved average absorption value in the whole visible spectrum range (370−880 nm) is up to 83%. These features make it a near-perfect ultrathin black absorber. The optical photo for the structure (size scale of 2 × 2 cm^2) shown in Figure 1b confirms the real black absorber achieved by this simple design and facile fabrication process.

Figure 2 shows the structural features of the meta-surface structures with different nominal thickness via the field-emission scanning electron microscopy (FE-SEM) technique. With the nominal thickness of 2 nm, the formed meta-surface structure shows a pattern of densely packed nanoparticles (size ∼15 nm) in Figure 2a,b. For the situation of a 4-nm-thick meta-surface, the nanoparticles grow to larger nanoparticles (size ∼30 nm) with various shapes as shown in Figure 2c,d. For the case of a 7-nm-thick meta-surface, nanoclusters are formed as a result of the combination of different nanoparticles as shown in Figure 2e,f. The metallic clusters grown with wide size distribution could provide a series of plasmon resonances located at different optical frequencies. In particular, the automatically formed ultranarrow gaps (less than 10 nm) between the adjacent clusters or between the face-to-face parts of the crossing cluster provide efficient plasmon near-field coupling and hybridization of the dipolar plasmon resonances.[45−47] As a result, a broadened and enhanced light absorption spectrum is then achieved. For the situation of a 9-nm-thick meta-surface, the nanoclusters touch each other and form the porous metal film as shown in Figure 2g,h. By further increasing the deposition time, the continuous metal film without holes could be achieved. Nevertheless, the continuous

DOI: 10.1021/acsami.5b00056
ACS Appl. Mater. Interfaces 2015, 7, 4962−4968

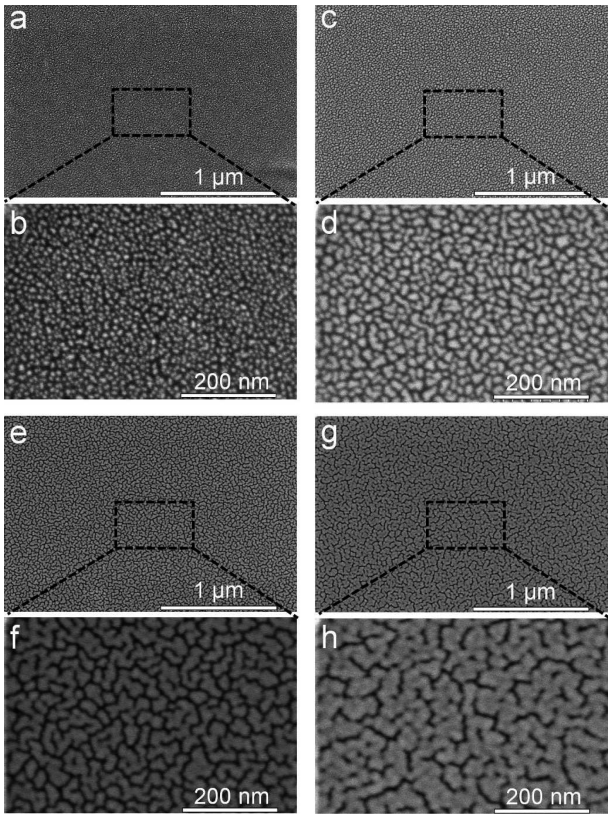

Figure 2. FE-SEM images of the metallic film-formation structures with different nominal thickness values of 2 nm (a, b), 4 nm (c, d), 7 nm (e, f), and 9 nm (g, h), respectively.

metal film without light-plasmon interaction resonators, such as nanoparticles or nanoscale gaps, leads to the inefficient light coupling and the high reflectivity.

Tuning the Light Absorption Properties. To understand the absorption properties of this meta-surface-based structure, a series of PMAs with different structural parameters have been fabricated by tuning the film thicknesses of the Au meta-surface layer and the dielectric spacer. The measured reflection of the fabricated PMAs with a stable meta-surface thickness but with a tuning spacer thickness (t) is plotted and shown in Figure 3. The PMA with a 4-nm-thick meta-surface shows a multispectral absorption behavior by tuning the spacer thickness from 10 to 100 nm (Figure 3a). With t = 20 and 40 nm, the spectral curves show broadband absorption behaviors. Figure 3b presents the absorption properties of the PMAs with a 7-nm-thick meta-surface under a varying t of the spacer. With increasing t, a clear evolution process of the light absorption modulation is observed. A continuously enhanced light absorption emerges in a broad spectral range (from 415 to 830 nm) with increasing t from 10 to 40 nm. The high light absorption is then weakened in the whole spectral range, especially in the short-wavelength regime, when t keeps increasing to 60 and 100 nm. This could be the main result of the broken-down near-field coupling between the meta-surface and the metal substrate. Thereby, for the PMA with a thick spacer, the strongly weakened coupling of dipolar plasmon resonances of the top metal-surface to their images in the bottom metallic mirror would limit the light absorption behavior to only occur in discrete wavelength ranges, where the certain optical interference is supported by the dielectric waveguide layer.[30] For the structure with a thicker meta-surface layer (9 nm), with increasing t of the spacer, two obvious light absorption evolution processes are observed in Figure 3c. One is the continuous red-shift of the resonant absorption spectrum curves. The other is the increase of the absorption intensity within the narrowband spectrum. The narrowed absorption bandwidth is due to the extremely reduced plasmon resonances of the meta-surface since the metallic porous film is already formed (Figure 2h). For the situation of the structure with a nearly complete continuous metal film (12 nm), the obvious resonant absorption band is observed in the spectrum (Figure 3d). During the increasing of the t, in comparison with the absorption behaviors of the

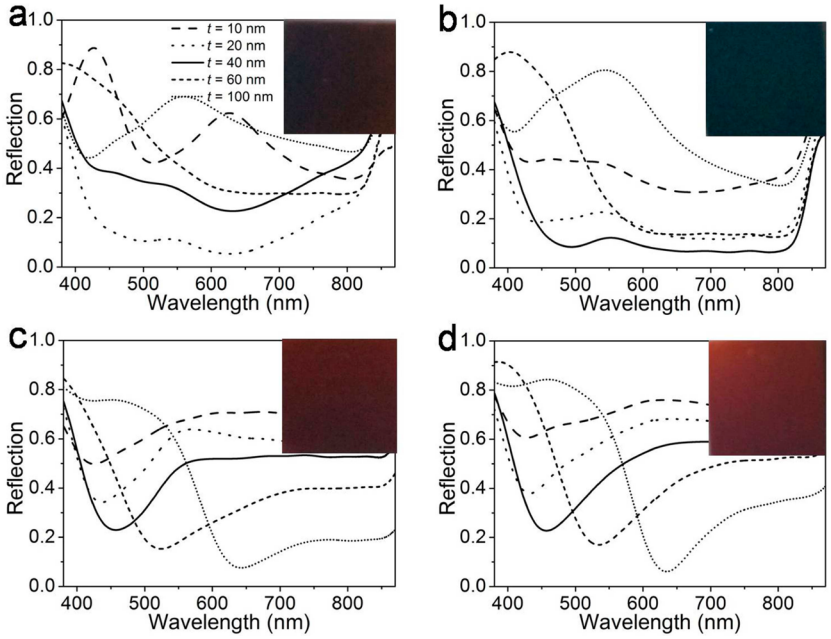

Figure 3. Reflection evolution spectra of the PMA with different certain thicknesses of the top metallic film of 4 nm (a), 7 nm (b), 9 nm (c), and 12 nm (d) via tuning the thickness of the SiO_2 spacer, respectively.

DOI: 10.1021/acsami.5b00056
ACS Appl. Mater. Interfaces 2015, 7, 4962−4968

structure with a porous metal film, a similar spectral evolution with a continuously enhanced light absorption and a simultaneous red-shift within a much narrower bandwidth is observed. For the structure with a complete metal film, this light absorption shows obvious degeneration from broadband absorption by the former metallic nanoparticle meta-surface to narrowband absorption of the typical MIM absorber. Therefore, highly tunable light absorption features of the proposed PMAs are obtained by tuning the thickness of the spacer layer and the geometry characteristics of the meta-surface.

By setting the thickness values of both the meta-surface and the spacer layer, a series of PMAs with different reflection colors could be observed. In order to do a direct comparison of these PMAs, we fabricate a variety of PMAs integrated on quartz (2×2 cm^2) by controlling the sputtering deposition time to produce certain metal and dielectric films. As a result, the visualized PMAs with color responses corresponding to their structural features are observed in Figure 4. For instance,

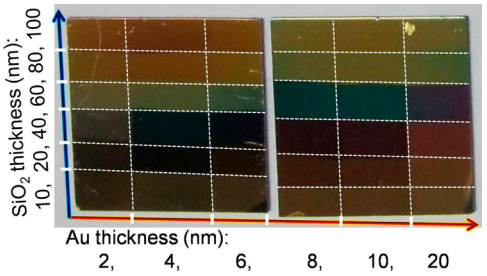

Figure 4. Photograph of proposed absorber under different structural parameters and the plotted diagram for the structures under certain thickness values of the Au meta-surface and SiO_2 spacer. The size of the square piece is 2×2 cm^2.

for the structures with a 4- or 6-nm-thick meta-surface, the PMAs provide broadband light absorption and result in the nearly black image when the SiO_2 spacer is in the thickness range from 20 to 40 nm. This is the main result of the simultaneous existence of multiple plasmon resonances by the wide size scale nanoparticles and the efficiently cooperative effects of the plasmon near-field coupling as well as the efficient plasmon magnetic resonances occurring between the top metasurface and the bottom reflector.[9−12] For the structures with a stable spacer thickness, the light absorption properties could be highly tuned via varying the meta-surface thickness as well. Overall, it is observed that the efficient light absorption achieved is with high tunability via controlling the structural features.

Resonant Electromagnetic Properties. To understand the mechanism of the experimentally observed broadband light absorption, the three-dimensional finite-difference time-domain method has been used to calculate the spectral response and the optical field behaviors. Here we take the PMA structure with a 7-nm-thick meta-surface and a 40-nm-thick SiO_2 spacer on a 100 nm gold mirror as an example to study the absorption mechanism. Simplified meta-surface structure with a hexagonal crystal consisting of densely packed gold square cubes is used to model the metallic nanostructures qualitatively. The side length and the height of the cube are 40 and 7 nm, respectively. The gap distance between the adjacent cubes is 6 nm. These values are close to those of the experimental average sizes.

Figure 5 presents the calculated light absorption spectrum and the corresponding optical field distributions at the resonant

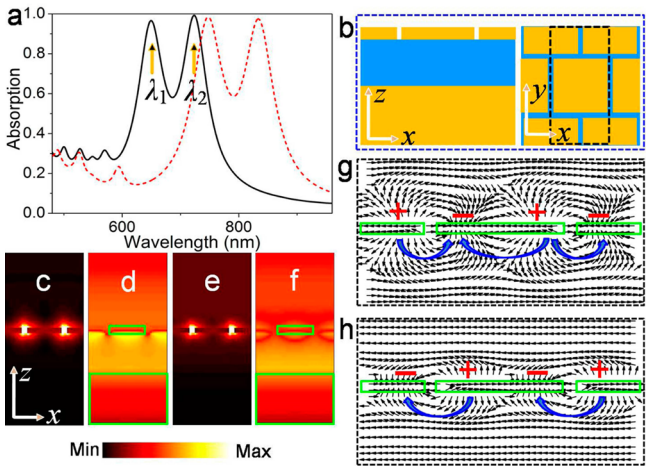

Figure 5. (a) Calculated absorption spectrum of the PMA composed of a 7 nm Au film deposited on a 100 nm gold film with a 40 nm SiO_2 spacer layer, where the modeling cube is with a side length of 40 nm (solid line) or 60 nm (dashed line). (b) Schematic of the model with a hexagonal-packed cube array. (c,d) Normalized electric and magnetic field distribution patterns at λ_1, respectively. (e,f) Normalized electric and magnetic field distribution patterns at λ_2, respectively. (g,h) Vector current mappings at λ_1 and λ_2, respectively.

wavelengths. In contrast to the single resonant absorption peak of the conventional MIM absorber with a large gap distance between the adjacent metallic particles,[7] a dual-band strong light absorption[48] is observed (solid line in Figure 5a) for the proposed modeling structure with particles packed in close proximity as shown in Figure 5b. In addition, the absorption of the structure with a larger cube array (side length of 60 nm) is also presented in Figure 5a (dashed line) with an obviously red-shifted dual-band absorption curve. This finding confirms the high tunability of the absorption spectrum via controlling the structural size. Thereby, for the experimental structure with wide size distributions of the metallic nanoparticles and the spatially distributed gap distances between the adjacent nanoclusters, the collective contributions from these subsystems with their own light absorption occurring in different wavelength ranges produce an extremely expanded absorption spectrum, as the real experimental results above show.

For the observed dual-band absorption phenomenon, the further calculated normalized electronic field intensity and magnetic field distribution patterns of the absorption peaks (λ_1 and λ_2) are presented to understand the double resonant absorption behaviors. At λ_1, as the normalized electric field intensity distribution shows in Figure 5c, strong confined electric field is observed in the areas close to the tips of the cubes, suggesting the excitation of the plasmon resonances by the meta-surface. The magnetic field pattern (Figure 5d) presents a strong field distributed in the spacer area and the area close to the cubes, which indicates the strong plasmon polariton with the induced plasmonic magnetic resonance within the dielectric layer sandwiched by the top meta-surface and the bottom mirror. For the absorption peak at λ_2, strong electric field intensity distributed around the cubes is also observed (Figure 5e). Nevertheless, in comparison with the magnetic field distribution at λ_1, only a quite weak magnetic field distribution is observed along the cubes for the absorption band at λ_2 (Figure 5f). These results suggest that the contributions for this absorption band could be provided by

DOI: 10.1021/acsami.5b00056
ACS Appl. Mater. Interfaces 2015, 7, 4962−4968

the similar plasmon polariton effects and the probably different plasmon resonances.

To get a better insight on these features, the current mapping at these absorption peaks is presented in Figure 5g,h for λ_1 and λ_2, respectively. The strong current circulating from one side of the cube to the other side (as the blue arrow marked in Figure 5g) suggests efficient excitation of the particle plasmon resonance of the cube itself.[39,54] The symbols "+" and "−" show the positive and negative current charges, respectively. The partial currents crossing the gaps between the adjacent cubes indicate excitation of the plasmon near-field coupling resonance.[46] Thereby, the absorption at λ_1 is mainly due to the excitations of the particle plasmons and the plasmon near-field coupling between the adjacent particles. At λ_2, the current mapping shows strong crossing current patterns between the adjacent cubes as the blue arrows marked in Figure 5h. This feature confirms the efficient excitation of the strong plasmon near-field coupling between the cubes packed in close proximity.[39,44] Thereby, for the proposed PMA in our scheme, besides the conventional plasmon polariton effects by metallo-dielectric structure similar to that of the conventional metamaterial MIM absorber,[12] the unique strong plasmon resonances including the particle plasmon resonances and the plasmon near-field coupling resonances based on the metallic particles packed in close proximity[44−51,54] are with significant contributions.

CONCLUSIONS

In summary, this paper presented a new and simplified approach for achieving near-perfect broadband light absorbers. The proposed PMA is based on the conventional opaque metal mirror and the dielectric spacer but with a unique plasmonic meta-surface structure. The light absorption properties can be efficiently manipulated via tuning the structural parameters including the norminal thicknesses of the meta-surface and the spacer layer. The experimentally achieved broadband light absorption phenomenon has been theoretically discussed by modeling the real meta-surface structure to be a simplified uniform hexagonally packed plasmonic crystal. Calculation results confirm that the broadband light absorption main be attributed to the plasmon resonances including the strong plasmon near-field coupling resonances, the particle plasmon resonances, together with the typical plasmon polariton effects. These results also confirm that an ultrathin meta-surface layer (less than 10 nm) structure can produce nearly ideal broadband light absorption with well-controlled bandwidth via tuning the structural parameters, paving the feasible way for a variety of highly customizable optical absorbers. In particular, the presented absorber can be obtained automatically during the sputtering deposition without any requirements of artificially precise design or multiple-process controlling. The only technical operation is to control the deposition time, which should be set to a certain value before the deposition. These novel optical properties as well as the impressive structural features including the quite simple and cost-effective fabrication technique make the proposed PMA an outstanding candidate for advanced high-efficiency absorber materials.

AUTHOR INFORMATION

Corresponding Authors

*E-mail: zliu@jxnu.edu.cn. Tel.: +86 0791 8812 2390. Fax: +86 0791 8812 2390.

*E-mail: liugq@jxnu.edu.cn.

Notes

The authors declare no competing financial interest.

ACKNOWLEDGMENTS

The authors acknowledge support from National Natural Science Foundation of China (Grants 11464019, 11264017 and 11304159), Natural Science Foundation of Jiangxi Province (Grant 20142BAB212001), Young Scientist Development Program of Jiangxi Province (Grant 20142BCB23008), Project of Jiangxi Provincial Education Department (Grant GJJ14253) and Key Projects of Jiangxi Normal University (Grants 6047, 5460).

REFERENCES

(1) Chen, K.; Adato, R.; Altug, H. Dual-Band Perfect Absorber for Multispectral Plasmon-Enhanced Infrared Spectroscopy. *ACS Nano* **2012**, *6*, 7998−8006.

(2) Liu, N.; Mesch, M.; Weiss, T.; Hentschel, M.; Giessen, H. Infrared Perfect Absorber and Its Application as Plasmonic Sensor. *Nano Lett.* **2010**, *10*, 2342−2348.

(3) Tittl, A.; Mai, P.; Taubert, R.; Dregely, D.; Liu, N.; Giessen, H. Palladium-Based Plasmonic Perfect Absorber in the Visible Wavelength Range and Its Application to Hydrogen Sensing. *Nano Lett.* **2011**, *11*, 4366−4369.

(4) Aydin, K.; Ferry, V. E.; Briggs, R. M.; Atwater, H. A. Broadband Polarization-Independent Resonant Light Absorption Using Ultrathin Plasmonic Super Absorbers. *Nat. Commun.* **2011**, *2*, 517.

(5) Chen, X.; Chen, Y.; Yan, M.; Qiu, M. Nanosecond Photothermal Effects in Plasmonic Nanostructures. *ACS Nano* **2012**, *6*, 2550−2557.

(6) Li, W.; Valentine, J. Metamaterial Perfect Absorber Based Hot Electron Photodetection. *Nano Lett.* **2014**, *14*, 3510−3514.

(7) Landy, N. I.; Sajuyigbe, S.; Mock, J. J.; Smith, D. R.; Padilla, W. J. Perfect Metamaterial Absorber. *Phys. Rev. Lett.* **2008**, *100*, 207402.

(8) Liu, X.; Starr, T.; Starr, A. F.; Padilla, W. J. Infrared Spatial and Frequency Selective Metamaterial with Near-Unity Absorbance. *Phys. Rev. Lett.* **2010**, *104*, 207403.

(9) Hao, J.; Wang, J.; Liu, X.; Padilla, W. J.; Zhou, L.; Qiu, M. High Performance Optical Absorber based on a Plasmonic Metamaterial. *Appl. Phys. Lett.* **2010**, *96*, 251104.

(10) Watts, C. M.; Liu, X.; Padilla, W. J. Metamaterial Electromagnetic Wave Absorbers. *Adv. Mater.* **2012**, *24*, OP98−OP120.

(11) Cui, Y.; He, Y.; Jin, Y.; Ding, F.; Yang, L.; Ye, Y.; Zhong, S.; Lin, Y.; He, S. Plasmonic and Metamaterial Structures as Electromagnetic Absorbers. *Laser Photonics Rev.* **2014**, *8*, 495−520.

(12) Jiang, Z. H.; Yun, S.; Toor, F.; Werner, D. H.; Mayer, T. S. Conformal Dual-Band Near-Perfectly Absorbing Mid-Infrared Metamaterial Coating. *ACS Nano* **2011**, *5*, 4641−4647.

(13) Wang, J.; Fan, C.; Ding, P.; He, J.; Cheng, Y.; Hu, W.; Cai, G.; Liang, E.; Xue, Q. Tunable Broad-Band Perfect Absorber by Exciting of Multiple Plasmon Resonances at Optical Frequency. *Opt. Express* **2012**, *20*, 14871−14878.

(14) Cui, Y.; Xu, J.; Fung, K. H.; Jin, Y.; Kumar, A.; He, S.; Fang, N. X. A Thin Film Broadband Absorber based on Multi-sized Nanoantennas. *Appl. Phys. Lett.* **2011**, *99*, 253101.

(15) Wang, W.; Cui, Y.; He, Y.; Hao, Y.; Lin, Y.; Tian, X.; Ji, T.; He, S. Efficient Multiband Absorber based on One-Dimensional Periodic Metal−Dielectric Photonic Crystal with a Reflective Substrate. *Opt. Lett.* **2014**, *39*, 331−334.

(16) Cui, Y.; Fung, K. H.; Xu, J.; Ma, H.; Jin, Y.; He, S.; Fang, N. X. Ultrabroadband Light Absorption by a Sawtooth Anisotropic Metamaterial Slab. *Nano Lett.* **2012**, *12*, 1443−1447.

(17) Zhou, J.; Kaplan, A. F.; Chen, L.; Guo, L. J. Experiment and Theory of the Broadband Absorption by a Tapered Hyperbolic Metamaterial Array. *ACS Photonics* **2014**, *1*, 618−624.

(18) Liang, Q.; Wang, T.; Lu, Z.; Sun, Q.; Fu, Y.; Yu, W. Metamaterial-Based Two Dimensional Plasmonic Subwavelength

DOI: 10.1021/acsami.5b00056
ACS Appl. Mater. Interfaces 2015, 7, 4962−4968

Structures Offer the Broadest Waveband Light Harvesting. *Adv. Opt. Mater.* **2013**, *1*, 43−49.
(19) Yang, J.; Hu, X.; Li, X.; Liu, Z.; Liang, Z.; Jiang, X.; Zi, J. Broadband Absorption Enhancement in Anisotropic Metamaterials by Mirror Reflections. *Phys. Rev. B* **2009**, *80*, 125103.
(20) Moreau, A.; Ciracì, C.; Mock, J. J.; Hill, R. T.; Wang, Q.; Wiley, B. J.; Chilkoti, A.; Smith, D. R. Controlled-Reflectance Surfaces with Film-Coupled Colloidal Nanoantennas. *Nature* **2012**, *492*, 86−89.
(21) Argyropoulos, C.; Le, K. Q.; Mattiucci, N.; D'Aguanno, G.; Alù, A. Broadband Absorbers and Selective Emitters based on Plasmonic Brewster Metasurfaces. *Phys. Rev. B* **2013**, *87*, 205112.
(22) Teperik, T. V.; García de Abajo, F. J.; Borisov, A. G.; Abdelsalam, M.; Bartlett, P. N.; Sugawara, Y.; Baumberg, J. J. Omnidirectional Absorption in Nanostructured Metal Surfaces. *Nat. Photonics* **2008**, *2*, 299−301.
(23) Thongrattanasiri, S.; Koppens, F. H. L.; García de Abajo, F. J. Complete Optical Absorption in Periodically Patterned Grapheme. *Phys. Rev. Lett.* **2012**, *108*, 047401.
(24) Liu, Z.; Zhan, P.; Chen, J.; Tang, C.; Yan, Z.; Chen, Z.; Wang, Z. Dual Broadband Near-Infrared Perfect Absorber based on a Hybrid Plasmonic-Photonic Microstructure. *Opt. Express* **2013**, *21*, 3021−3030.
(25) Hedayati, M. K.; Javaherirahim, M.; Mozooni, B.; Abdelaziz, R.; Tavassolizadeh, A.; Chakravadhanula, V. S. K.; Zaporojtchenko, V.; Strunkus, T.; Faupel, F.; Elbahri, M. Design of a Perfect Black Absorber at Visible Frequencies Using Plasmonic Metamaterials. *Adv. Mater.* **2011**, *23*, 5410−5414.
(26) De Volder, M. F. L.; Tawfick, S. H.; Baughman, R. H.; Hart, A. J. Carbon Nanotubes: Present and Future Commercial Applications. *Science* **2013**, *339*, 535−539.
(27) Geldmeier, J.; König, T.; Mahmoud, M. A.; El-Sayed, M. A.; Tsukruk, V. V. Tailoring the Plasmonic Modes of a Grating-Nanocube Assembly to Achieve Broadband Absorption in the Visible Spectrum. *Adv. Funct. Mater.* **2014**, *24*, 6797−6805.
(28) Hägglund, C.; Zeltzer, G.; Ruiz, R.; Thomann, I.; Lee, H. B. R.; Brongersma, M. L.; Bent, S. F. Self-Assembly Based Plasmonic Arrays Tuned by Atomic Layer Deposition for Extreme Visible Light Absorption. *Nano Lett.* **2013**, *13*, 3352−3357.
(29) Hirsch, L. R.; Stafford, R.; Bankson, J.; Sershen, S.; Rivera, B.; Price, R.; Hazle, J.; Halas, N.; West, J. Nanoshell-Mediated Near-Infrared Thermal Therapy of Tumors under Magnetic Resonance Guidance. *Proc. Natl. Acad. Sci. U.S.A.* **2003**, *100*, 13549−13554.
(30) Neumann, O.; Urban, A. S.; Day, J.; Lal, S.; Nordlander, P.; Halas, N. J. Solar Vapor Generation Enabled by Nanoparticles. *ACS Nano* **2012**, *7*, 42−49.
(31) Lenert, A.; Bierman, D. M.; Nam, Y.; Chan, W. R.; Celanović, I.; Soljačić, M.; Wang, E. N. A Nanophotonic Solar Thermophotovoltaic Device. *Nat. Nanotechnol.* **2014**, *9*, 126−130.
(32) Taflove, A.; Hagness, S. C. Computational Electrodynamics: The Finite-Difference Time Domain Method; Artech House, Inc.: Norwood, MA, 2005.
(33) Palik, E. D. Handbook of Optical Constants of Solids; Academic: Orlando, FL, 1985.
(34) Chen, J.; Xu, R.; Liu, Z.; Tang, C.; Chen, Z.; Wang, Z. Fabrication and Infrared-Transmission Properties of Monolayer Hexagonal-Close-Packed Metallic Nanoshells. *Opt. Commun.* **2013**, *297*, 194−197.
(35) Søndergaard, T.; Novikov, S. M.; Holmgaard, T.; Eriksen, R. L.; Beermann, J.; Han, Z.; Pedersen, K.; Bozhevolnyi, S. I. Plasmonic Black Gold by Adiabatic Nanofocusing and Absorption of Light in Ultra-Sharp Convex Grooves. *Nat. Commun.* **2012**, *3*, 969.
(36) Li, Z.; Butun, S.; Aydin, K. Ultranarrow Band Absorbers Based on Surface Lattice Resonances in Nanostructured Metal Surfaces. *ACS Nano* **2014**, *8*, 8242−8248.
(37) Wu, C.; Neuner, B.; Shvets, G.; John, J.; Milder, A.; Zollars, B.; Savoy, S. Large-Area Wide-Angle Spectrally Selective Plasmonic Absorber. *Phys. Rev. B* **2011**, *84*, 075102.
(38) Oates, T. W. H.; Mücklich, A. Evolution of Plasmon Resonances during Plasma Deposition of Silver Nanoparticles. *Nanotechnology* **2005**, *16*, 2606.
(39) Schuller, J. A.; Barnard, E. S.; Cai, W.; Jun, Y. C.; White, J. S.; Brongersma, M. L. Plasmonics for Extreme Light Concentration and Manipulation. *Nat. Mater.* **2010**, *9*, 193−204.
(40) Zhan, P.; Wang, Z. L.; Dong, H.; Sun, J.; Wang, H. T.; Zhu, S. N.; Ming, N. B.; Zi, J. The Anomalous Infrared Transmission of Gold Films on Two-Dimensional Colloidal Crystals. *Adv. Mater.* **2006**, *18*, 1612−1616.
(41) Atwater, H. A.; Polman, A. Plasmonics for Improved Photovoltaic Devices. *Nat. Mater.* **2010**, *9*, 205−213.
(42) Liu, Z.; Hang, J.; Chen, J.; Yan, Z.; Tang, C.; Chen, Z.; Zhan, P. Optical Transmission of Corrugated Metal Films on a Two-Dimensional Hetero-Colloidal Crystal. *Opt. Express* **2012**, *20*, 9215−9225.
(43) Beyene, H. T.; Tichelaar, F. D.; Verheijen, M. A.; van de Sanden, M. C. M.; Creatore, M. Plasma-Assisted Deposition of Au/SiO_2 Multi-layers as Surface Plasmon Resonance-Based Red-Colored Coatings. *Plasmonics* **2011**, *6*, 255−260.
(44) Le, F.; Brandl, D. W.; Urzhumov, Y. A.; Wang, H.; Kundu, J.; Halas, N. J.; Aizpurua, J.; Nordlander, P. Metallic Nanoparticle Arrays: A Common Substrate for Both Surface-Enhanced Raman Scattering and Surface-Enhanced Infrared Absorption. *ACS Nano* **2008**, *2*, 707−718.
(45) Wang, H.; Brandl, D. W.; Nordlander, P.; Halas, N. J. Plasmonic Nanostructures: Artificial Molecules. *Acc. Chem. Res.* **2007**, *40*, 53−62.
(46) Halas, N. J.; Lal, S.; Chang, W. S.; Link, S.; Nordlander, P. Plasmons in Strongly Coupled Metallic Nanostructures. *Chem. Rev.* **2011**, *111*, 3913−3961.
(47) Prodan, E.; Radloff, C.; Halas, N. J.; Nordlander, P. A Hybridization Model for the Plasmon Response of Complex Nanoparticles. *Science* **2003**, *302*, 419−422.
(48) Atay, T.; Song, J. H.; Nurmikko, A. V. Strongly Interacting Plasmon Nanoparticle Pairs: From Dipole−Dipole Interaction to Conductively Coupled Regime. *Nano Lett.* **2004**, *4*, 1627−1631.
(49) Su, K.-H.; Wei, Q.-H.; Zhang, X.; Mock, J. J.; Smith, D. R.; Schultz, S. Interparticle Coupling Effects on Plasmon Resonances of Nanogold Particles. *Nano Lett.* **2003**, *3*, 1087−1090.
(50) Liu, Z.; Liu, G.; Zhou, H.; Liu, X.; Huang, K.; Chen, Y.; Fu, G. Near-Unity Transparency of a Continuous Metal Film via Cooperative Effects of Double Plasmonic Arrays. *Nanotechnology* **2013**, *24*, 155203.
(51) Aćimović, S. S.; Kreuzer, M. P.; González, M. U.; Quidant, R. Plasmon Near-Field Coupling in Metal Dimers as a Step toward Single-Molecule Sensing. *ACS Nano* **2009**, *3*, 1231−1237.
(52) Verellen, N.; Dorpe, P. V.; Huang, C.; Lodewijks, K.; Vandenbosch, G. A. E.; Lagae, L.; Moshchalkov, V. V. Plasmon Line Shaping Using Nanocrosses for High Sensitivity Localized Surface Plasmon Resonance Sensing. *Nano Lett.* **2011**, *11*, 391−397.
(53) Enoch, S.; Quidant, R.; Badenes, G. Optical Sensing based on Plasmon Coupling in Nanoparticle Arrays. *Opt. Express* **2004**, *12*, 3422−3427.
(54) Liu, Z.; Shao, H.; Liu, G.; Liu, X.; Zhou, H.; Hu, Y.; Zhang, X.; Cai, Z.; Gu, G. $\lambda^3/20000$ Plasmonic Nanocavities with Multispectral Ultra-Narrowband Absorption for High-Quality Sensing. *Appl. Phys. Lett.* **2014**, *104*, 081116.
(55) König, M.; Rahmani, M.; Zhang, L.; Lei, D. Y.; Roschuk, T. R.; Giannini, V.; Qiu, C. W.; Hong, M.; Schlücker, S.; Maier, S. A. Unveiling the Correlation between Nanometer-Thick Molecular Monolayer Sensitivity and Near-Field Enhancement and Localization in Coupled Plasmonic Oligomers. *ACS Nano* **2014**, *8*, 9188−9198.
(56) Shen, Y.; Zhou, J.; Liu, T.; Tao, Y.; Jiang, R.; Liu, M.; Xiao, G.; Zhu, J.; Zhou, Z. K.; Wang, X.; Jin, C.; Wang, J. Plasmonic Gold Mushroom Arrays with Refractive Index Sensing Figures of Merit Approaching the Theoretical Limit. *Nat. Commun.* **2013**, *4*, 2381.

DOI: 10.1021/acsami.5b00056
ACS Appl. Mater. Interfaces 2015, 7, 4962−4968